Int J Adv Manuf Technol (2015) 77:1681–1701
DOI 10.1007/s00170-014-6450-y

ORIGINAL ARTICLE

Influence of thermal characteristics on microstructure of pulse current GMA weld bead of HSLA steel

B. P. Agrawal · P. K. Ghosh

Received: 12 April 2011 / Accepted: 29 September 2014 / Published online: 16 November 2014

Abstract The influence of pulse parameters of pulse current gas metal arc welding (P-GMAW) on thermal behavior of weld has been studied considering summarized influence of pulse parameters defined by a dimensionless factor $\phi=[(I_b/I_p)f.t_b]$, mean current (I_m), and heat input (Ω) during weld bead deposition on high-strength low-alloy steel plate using low-alloy steel filler wire. The thermal behavior of the weld has been estimated with the help of appropriate expressions. The validity of those estimations has been confirmed by comparing them with measured values and found that they are well in agreement to each other with a deviation lying in the range of 7 to 8 %. It is observed that variation in thermal characteristics of weld is maintaining good correlation with ϕ, I_m, and Ω of the welding process. The thermal characteristics of the weld are correlated to microstructure.

Keywords P-GMAW · Pulse parameters · Weld pool · HSLA steel · Weld isotherm, thermal cycle

B. P. Agrawal
School of Mechanical Engineering, Galgotias University, Greater Noida 201308, Gautam Budh Nagar, India
e-mail: banshiprasad@gmail.com

e-mail: banshi_agrawal@yahoo.com

P. K. Ghosh (✉)
Department of Metallurgical & Materials Engineering, Indian Institute of Technology Roorkee, Roorkee 247667, India
e-mail: prakgfmt@gmail.com

P. K. Ghosh
e-mail: prakgfmt@iitr.ernet.in

1 Introduction

Service performance of weld joint is largely dictated by the properties of weld, which is primarily governed by its chemical composition and microstructure. In this regard, control of weld characteristics especially becomes imperative in case of high-strength materials. In this context, it is remembered that growing demand of using high-strength low-alloy (HSLA) steel in welded structure often requires a clear understanding about the properties of weld metal resulting from its transformation of microstructure primarily depending upon thermal characteristics governed by the welding parameters [1–4]. The presence of coarse microstructure in weld is generally considered as one of the prime causes of its weakening [5]. Thus, to achieve superior properties of a weld joint, a control over the coarsening of microstructure of weld may be considered of great importance. Various techniques are used for this purpose which is largely known as vibration of solidifying weld pool, alloying addition as grain refiner in filler metal, control of heat input and thermal characteristics of weld [5], and lowering of heat built up in weld pool introducing interruption in its solidification using pulsed current [6]. The refining of microstructure of weld by minor alloying additions in filler wire of gas metal arc welding (GMAW) has been found significantly effective to improve the mechanical properties of weld joint. However, the use of pulsed current GMAW (P-GMAW) process has been found [7] to provide more improvement in mechanical properties of a weld containing grain refiner primarily by further refining its microstructure largely by the interruption in metal deposition under the pulsed current.

The interruption in metal deposition affecting the solidification of weld pool to refine its microstructure largely depends upon the pulse parameters affecting the thermal characteristics. Thus, a control over the thermal characteristics of the weld dictated by pulse parameters may have a considerable influence on microstructure of weld in P-GMAW process.

But, the selection of welding parameters in P-GMAW process is relatively more complicated than that found in case of conventional GMAW process due to involvement of large number of simultaneously interacting pulse parameters like peak current (I_p), base current (I_b), peak current duration (t_p), base current duration (t_b), and pulse frequency (f). However, solution to the difficulties of controlling the P-GMAW process has been successfully addressed [5–9] by introducing a summarized influence of pulse parameters defined by a dimensionless factor $\phi=[(I_b/I_p)f.t_b]$ proposed earlier, where t_b is expressed as $\left[\frac{1}{f}-t_p\right]$. This hypothetical factor has been derived from the energy balance concept of the process. The role of ϕ in understanding the effect of mean current (I_m), base current (I_b), pulse current (I_p), pulse time (t_p), and pulse frequency (f) on various characteristics of weld has been justified in earlier works [6, 10, 11]. But hardly any literature is readily available about the role of simultaneously interactive pulse parameters and their functions governing critically the thermal behavior of weld and weld isotherm, in case of P-GMAW of HSLA steel. The variation in thermal behavior of weld and weld isotherm consequently affects microstructure of the weld dictating the mechanical properties of the weld joint [12, 13]. Thus, an estimation of thermal characteristics defined by temperature of weld pool and weld isotherm prior to carrying out welding may be very much useful in controlling the welding process and procedure in order to achieve the desired quality of weld joint [8, 9, 14].

In view of the above, an effort has been made to study the effect of pulse parameters on thermal behavior of weld pool and weld isotherm as a function of ϕ during deposition of weld bead on HSLA steel plate using P-GMAW process. The thermal characteristics and weld isotherm have been estimated with the help of suitable expressions considering transfer of heat from two sources as welding arc and super heated metal droplets. The estimation of these thermal aspects has been verified with the help of experimentally measured values and further confirmed by their respective influence on microstructure of the weld and heat-affected zone (HAZ). The factor ϕ has been correlated to the thermal behavior of weld pool and weld isotherm.

2 Thermal characteristics

The heat input (Ω) of the welding process, total heat transferred to the weld pool (Q_T), and weld pool temperature (T_{WP}) at different distances from the fusion line as well as weld isotherm were estimated by using standard mathematical expressions as reported in various literatures [15–19].

2.1 Estimation of heat input

The Ω of P-GMAW processes as a function of mean current (I_m), arc voltage (V), and welding speed (S) has been estimated in consideration of arc efficiency (η_a) of the welding arc as follows [14, 16, 18].

$$\Omega = \frac{\eta_a \times V \times I_m}{S} \tag{1}$$

The I_m of P-GMAW process as a function of pulse parameters has been obtained [3, 14] as

$$I_m = \frac{(I_b t_b + I_p t_p)}{(t_b + t_p)} \tag{2}$$

For AWS A5.18: ER 70S-6 grade filler metal under argon gas shielding, the η_a of P-GMAW process has been considered as 70 % [20].

2.2 Estimation of total heat transferred to the weld pool ($\boldsymbol{Q}_T$)

The Q_T of P-GMAW processes has been estimated [15, 20] as a function of the arc heat transferred to the weld pool (Q_{AW}), heat transfer by deposition of superheated filler metal droplets to the weld pool (Q_f), and welding speed (S) as follows.

$$Q_T = \frac{(Q_{AW} + Q_f)}{S} \tag{3}$$

The Q_{AW} has been estimated using the expressions [15, 20] as

$$Q_{AW} = (V\, I_{eff} - \psi\, I_{eff})\eta_a \tag{4}$$

Where ψ and I_{eff} are the effective melting potential at anode and effective current (root mean square value of the pulsed current wave form), respectively. The I_{eff} is estimated [18, 21] using the following expression.

$$I_{eff} = \sqrt{\left[k_p.I_p^2 + (1-k_p).I_b^2\right]} \tag{5}$$

Where the pulse duty cycle,

$$k_p = {}^{t_p}/_{t_{pul}} \tag{6}$$

The Q_f has been estimated [15, 20] as follows

$$Q_f = Q_{de}\, m_t\, f \tag{7}$$

Where m_t is mass of filler wire transferred per pulse (kg), Q_{de} is heat content per unit mass of the filler wire (J kg^{-1}) at the time of deposition, and f is pulse frequency (Hz). The modeling part in detail for estimation of Q_f of P-GMAW process has been reported elsewhere [15, 20].

2.3 Estimation of weld pool temperature (T_{WP}) and weld isotherm

The T_{WP} of P-GMAW processes has been estimated considering the temperature rise (T_{arc}) at the point ($x(\xi)$, y, z) due to arc heating (Fig. 1) to the weld pool taking into account it as double ellipsoidal heat source [22–24] and temperature rise (T_{filler}) due to transfer of heat by superheated droplets of filler metal to the weld pool (Q_f) [17] as follows.

$$T_{WP} = T_{arc} + T_{filler} \tag{8}$$

The temperature rise (T_{arc}) arising out of arc heating can be expressed as follows [22, 23].

$$T_{arc} = \frac{3\sqrt{3}.Q_{AW}}{\rho.c.\pi\sqrt{\pi}}\int_0^t \left[\frac{dt'}{\sqrt{\left(12a(t-t') + a_h^2\right)}.\sqrt{\left(12a(t-t') + b_h^2\right)}}. \left(\frac{A'}{\sqrt{\left(12a(t-t') + c_{hf}^2\right)}} + \frac{B'}{\sqrt{\left(12a(t-t') + c_{hb}^2\right)}} \right) \right] + T_0 \tag{9}$$

Where Q_{AW}, ρ, c, a, T_0, and a_h, b_h, c_{hf}, c_{hb} are the arc heat transferred to the weld pool, mass density of the base metal, specific heat of the base metal, thermal diffusivity of the base metal, initial preheated temperature of groove wall, and the rests are ellipsoidal heat source parameters (Fig. 1), respectively.

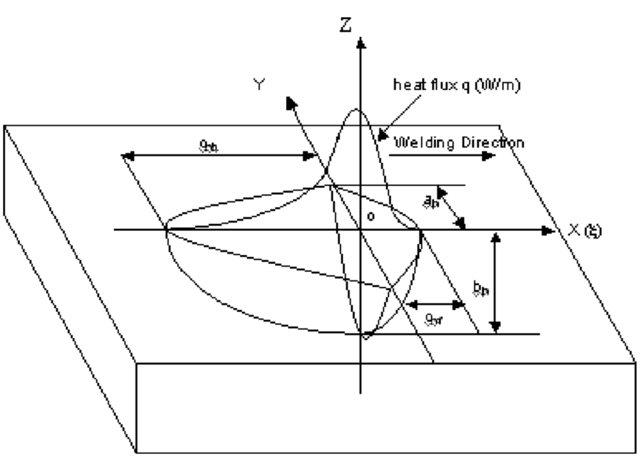

Fig. 1 Schematic diagram of double ellipsoidal heat source (volumetric heat source)

$$A' = r_f.\exp\left(-\frac{3(x-v.t')^2}{12a(t-t') + c_{hf}^2} - \frac{3\left(a/2\right)^2}{12a(t-t') + a_h^2} - \frac{3d^2}{12a(t-t') + b_h^2} \right) \tag{10}$$

$$B' = r_b.\exp\left(-\frac{3(x-v.t')^2}{12a(t-t') + c_{hb}^2} - \frac{3\left(a/2\right)^2}{12a(t-t') + a_h^2} - \frac{3d^2}{12a(t-t') + b_h^2} \right) \tag{11}$$

Where r_f and r_b are the proportion coefficients in front and behind the heat source, estimated as

$$r_f = {}^{2.c_{hf}}/_{(c_{hf} + c_{hb})} \tag{12}$$

$$r_b = {}^{2.c_{hb}}/_{(c_{hf} + c_{hb})} \tag{13}$$

The heat source parameter c_{hf} in front of the heat source and c_{hb} behind the arc may be considered as $c_{hf}=a_h$ and $c_{hb}=2\ c_{hf}$.

The arc heat transferred to the weld pool, Q_{AW}, can be estimated as

$$Q_{AW} = (V.I_{eff} - \psi.I_{eff}).\eta_a \tag{14}$$

where ψ is the effective melting potential at anode and η_a is the arc heat transfer efficiency. The effective current, I_{eff}, is estimated by considering the root mean square of the pulsed current wave form as

$$I_{eff} = \sqrt{\left[k_p.I_p^2 + (1-k_p).I_b^2\right]} \tag{15}$$

where k_p is the pulse duty cycle defined as

$$k_p = {}^{t_p}/_{t_{pul}} \tag{16}$$

Where t_{pul} is the pulse cycle time estimated as

$$t_{pul} = t_p + t_b \tag{17}$$

Similarly, the temperature rise of weld pool (T_{filler}) from superheated filler metal [17] can be estimated by using the expressions as follows

$$T_{filler} = \frac{Q_f}{2.\pi.k} e^{-\lambda.v.\xi}. \left[\frac{e^{-\lambda.v.R}}{R_1} + \sum_{n=1}^{n=\infty} \left(\frac{e^{-\lambda.v.R_n}}{R_{1n}} + \frac{e^{-\lambda.v.R'_n}}{R'_{1n}} \right) \right] \tag{18}$$

where R_1, R_{1n}, and R'_{1n} are estimated as stated below.

$$R_1 = \sqrt{\xi^2 + y^2 + z^2} \quad (19)$$

$$R_{1n} = \sqrt{(2.n.d - z)^2 + \xi^2 + y^2} \quad (20)$$

$$R'_{1n} = \sqrt{(2.n.d + z)^2 + \xi^2 + y^2} \quad (21)$$

The heat transfer to the weld pool by superheated filler metal per pulse (H_{fp}) and per unit time (Q_f) are expressed as follows

$$H_{fp} = H_{de}.m_{tp} \quad (22)$$

$$Q_f = H_{de}.m_{tp}.f \quad (23)$$

where m_{tp} and f are the mass of the filler wire transferred per pulse [15] and pulse frequency, respectively.

The weld isotherm has been estimated using the expressions of Eq. 8 and studied as a function of I_m, ϕ, and Ω.

3 Experimentation

Bead on plate weld deposition was carried out by considering Ω, I_m, and ϕ as 8.2±0.3, 12.1±0.2, and 13.4±0.5 kJ/cm; 220±3, 240±2, and 265±4 A; and 0.04, 0.08, 0.15, and 0.25, respectively, whereas the arc voltage was kept as 28±1 V. A relatively low arc voltage creates instability in shielding jacket due to relatively low arc pressure [9]. A comparatively higher arc voltage of 28±1 V has been considered in the present investigation in order to maintain a relatively stable arc [8].

3.1 Weld bead deposition

Weld bead deposition using P-GMA welding was carried out with the help of 1.2-mm-diameter AWS A5.18: ER 70S filler wire on 16-mm-thick control rolled micro-alloyed HSLA steel plate of grade SAILMA-410HI/SA533 with welding power source ESAB Aristo 2000–LUD 450 UW direct current (D.C). The bead deposition was performed with the polarity of direct current electrode positive (DCEP) wherein electrode is connected to positive and workpiece to negative of the output of power source. During bead deposition, the plate was rigidly fixed in a fixture. The weld deposition was carried out in flat position by a vertically placed welding torch, which was moving on an automated trolley using different pulse parameters. For each set of pulse parameters, three weld beads were deposited. The characteristics of the weld bead are studied on all three beads in order to minimize the effect of random fluctuation in power supply. The chemical compositions of the base plate and the filler wire according to the test certificate and obtained using spark emission optical spectroscopy are shown in Table 1.

During bead deposition, the stand of distance between the nozzle and workpiece was maintained within 16–17 mm. Weld deposition was carried out at different pulse parameters by using commercial pure argon (99.98 %) as shielding gas at a flow rate of 18 L per minute. The pulse characteristics such as I_p, I_b, t_p, t_b, and f were measured with the help of a transient recorder (maximum resolution 1 MHz) fitted with the electrical circuit of the welding set up. The typical behavior of pulse wave form captured by the transient recorder during welding has been shown in Fig. 2. From pulse wave form, the pulse characteristics are obtained. The arc voltage and I_m were noted on the pulse characteristics recorded with the help of WMS 4000 software installed in a computer connected to the circuit of the welding power source. The measured arc voltage and the mean current I_m at varied pulse parameters giving rise to different ϕ considered in this work are presented in Table 2. The estimated Ω, Q_{AW}, and Q_f observed at different ϕ of varied pulse parameters have also been shown in Table 2.

3.2 Measurement of weld thermal behavior

The temperatures of the molten weld pool was measured during bead deposition by introducing Pt – (Pt-13 Rh) thermocouple from the bottom of the plate in two different locations at distances of about 40 and 80 mm from the run on position of weld deposition. It ensures stable weld pool temperature at different depths of 2.5 and 3.5 mm, respectively, from the weld surface along the weld center line as shown in Fig. 3a, b. The temperature was measured by computerized recording with a time interval of 0.01 s through a “Strain Buster” (decentralized strain/temperature measuring module). Prior to their use, the thermocouple and “strain buster” were calibrated using known source of heating within the practically required range of temperature of the study.

3.3 Studies on microstructure

The microstructure of weld under different pulse parameters was studied on the specimens collected from the stable part of weld deposition ensuring true representation of bead characteristics. The transverse section of bead on plate weld deposit was prepared using standard metallographic technique and etched with 2 % nital solution to reveal the microstructure.

Table 1 Chemical composition of base and filler materials used in weld bead on plate studies

Materials	Grade	Chemical composition (wt%)											
		C	Si	Mn	Cr	Cu	Nb	Ti	V	Al	P	S	CE
Base plate 16 mm thick (TC)	SAILMA-350HI/SA533	0.13	0.3	1.34	0.003	0.037	0.05	0.020	0.042	0.08	0.019	0.015	0.37
Base plate 16 mm thick (SEOS)	SAILMA-350HI/SA533	0.12	0.28	1.51	0.04	0.024	0.048	0.02	0.04	0.06	0.016	0.014	0.39
Filler wire 1.2 mm, dia (TC)	A5.18: ER 70S	0.1	0.9	1.6	–	0.2	–	–	–	–	0.02	0.02	0.38

TC test certificate, *SEOS* spark emission optical spectroscopy

The microstructure of weld deposit was studied under optical microscope.

The measurement of grain size of HAZ adjacent to fusion line is done with the help of linear intercept method (ASTM E112) [25]. The measurements were made on at least 21 randomly selected locations and the average was found to represent the grain size of HAZ of a given weld.

4 Results and discussions

Properties of weld joint are primarily governed by the microstructure of weld and HAZ at a prevailing thermal exposure. The extent of thermal exposure largely depends upon the nature of metal transfer and thermal behavior of the weld dictating size and shape of the weld isotherm and temperature of weld pool. The heat content of weld pool is largely dictated by its mass per unit length and temperature. Thus, they affect the weld thermal cycle and phase transformation of any location of weld joint and control properties of the weld and HAZ. A highly precise control of all these thermal aspects of welding can be addressed by using P-GMAW process regulated by summarized influence of pulse parameters defined by the factor ϕ because it may facilitates governing the weld characteristics including its microstructure [15, 20]. Accordingly, the nature of variation in thermal characteristics and weld isotherm as a function of ϕ, Ω, and I_m has been studied, an understanding of which may be beneficial in using P-GMAW to produce desired weld quality of preferred microstructure.

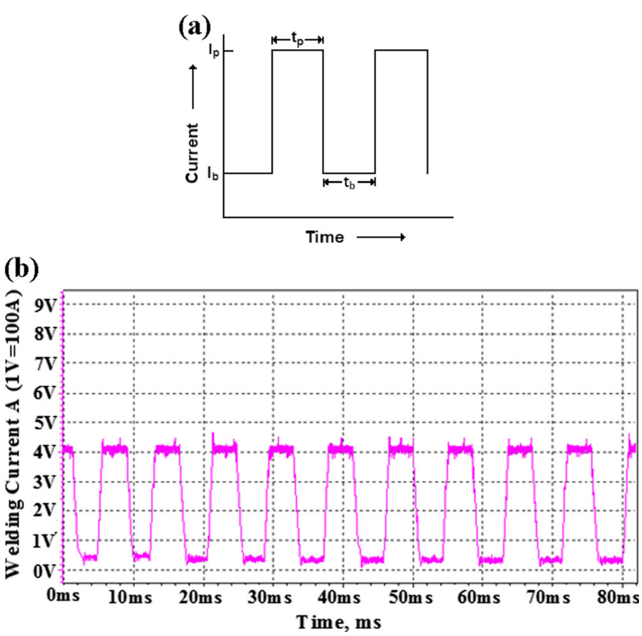

Fig. 2 Typical behavior of pulse current GMA welding at I_m=240 A, ϕ= 0.08 as observed in transient recorder

4.1 Thermal characteristics of metal transfer

At a given arc voltage of 28±1 V, the typical theoretically estimated thermal behavior of metal transfer as heat content per unit mass of droplet (Q_{de}) and temperature of droplet at the time of deposition (T_{de}) at different mean currents (I_m) of about 220±3, 240±2, and 265±4 A, where ϕ lying within the range of 0.04 to 0.25 has been shown in panels a and b of Fig. 4, respectively. It has been observed that the Q_{de} and T_{de} reduce with the increase of ϕ at a given I_m and vice versa. This is attributed to the heat gain by the droplet from energy input at the time of detachment from the electrode and heat loss by convection and radiation during its flight from electrode tip to the weld pool. For a given shielding gas and specific distance between the electrode and the workpiece, the heat loss during its flight from the electrode tip to the workpiece primarily depends upon the temperature of the droplet at the time of detachment from the electrode tip, surface area of the droplet, and flight time. An increase in the surface area of droplet enhances the heat loss whereas increment of velocity reduces the heat loss and vice versa. The surface area of droplet enhances with an increase of

Table 2 Pulse parameters and corresponding thermal behavior used in weld bead on plate deposition by P-GMAW process

Arc voltage (V)	Heat input (Ω) (kJ/cm)	Welding speed (S) (cm/min)	Mean current (I_m) (A)	I_{eff} (A)	ϕ	Pulse parameters					Thermal behavior	
						I_p (A)	I_b (A)	f (Hz)	t_b (s)	t_p (s)	Q_f (J/s)	Q_{AW} (J/s)
28±1	8.20±0.3	31.7	220±3	278	0.04	388	35	102	3.88	4.03	5,376	1,927
	12.1±0.2	21.4		259	0.08	357	67	104	3.87	4.01	4,981	1,835
	13.4±0.5	19.3		247	0.15	332	125	107	3.97	3.66	4,725	1,786
				234	0.24	295	164	106	4.07	3.51	4,576	1,760
	8.20±0.3	34.6	240±2	298	0.04	410	37	123	3.16	3.51	5,765	2,137
	12.1±0.2	23.3		288	0.08	377	84	125	2.73	3.55	5,372	2,042
	13.4±0.5	21.1		257	0.15	350	121	124	3.47	3.17	5,122	1,989
				242	0.25	316	164	126	3.84	3.01	4,989	1,966
	8.20±0.3	38.2	265±4	323	0.04	421	47	144	2.38	3.35	6,214	2,400
	12.1±0.2	25.8		296	0.08	393	75	142	2.66	3.27	5,811	2,298
	13.4±0.5	23.2		275	0.15	360	146	143	2.97	2.98	5,590	2,249
				268	0.25	322	190	145	2.55	2.88	5,509	2,234

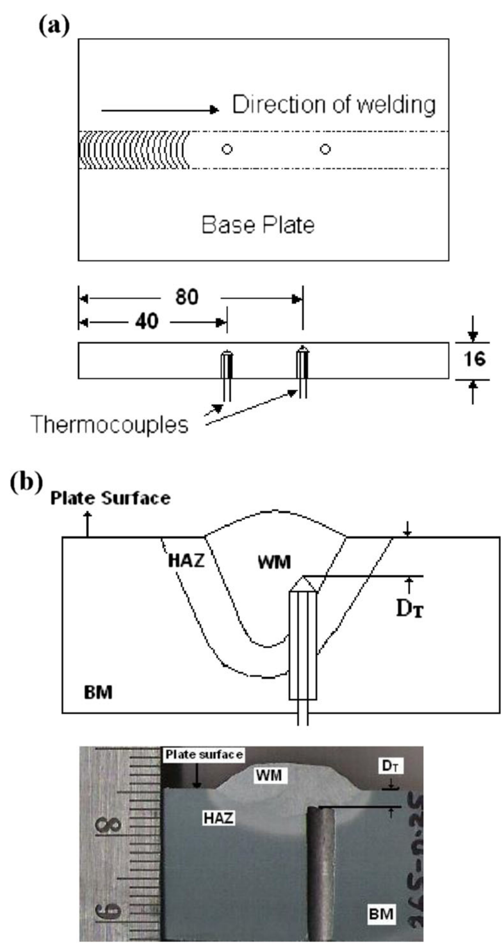

Fig. 3 **a** Schematic diagram showing location of thermocouples in bead on plate deposition. **b** Schematic diagram showing the depth of placement of thermocouple (D_T) and a typical corresponding macrograph of placement of thermocouple in weld pool

diameter of the droplet and number of droplets transferred per pulse and vice versa [20]. The diameter of droplets has been found to increase with increase of ϕ at a given I_m, and at a given ϕ, it reduces with the increase of I_m whereas, the number of droplets transferred per pulse reduces with the increase of ϕ at a given I_m or with the reduction of I_m at a given ϕ as shown in Fig. 5a, b. Thus, the surface area of droplets is governed by relative enhancement of the diameter of droplets and reduction in number of droplets transferred per pulse. It has been found that total heat loss decreases with the increase of ϕ at a given mean current, and at a given ϕ, it increases with an increase of mean current [15, 20]. The heat content of the droplet at the time of detachment has been found to reduce with an increase of ϕ at a given I_m and at a given ϕ with the enhancement of I_m [15, 20]. Considering all these facts, the Q_{de} and T_{de} depend upon the comparative rate of reduction of the heat content of droplet at the time of deposition and heat loss of the droplet during its flight from the electrode tip to the weld pool. Due to these reasons, the trend of Q_{de} and T_{de} has been found as shown in panels a and b of Fig. 4, respectively. Hence, it can be concluded that the thermal behavior of metal transfer can be controlled up to a certain extent by varying ϕ and I_m as stated in their empirical correlations given below.

$$Q_{de} = 302.71 - 0.34\, I_m - 219.66\phi + 0.46 I_m \phi + e_{r1} \quad (24)$$

$$T_{de} = 3934 - 4.26\, I_m - 2751\phi + 5.75 I_m \phi + e_{r2} \quad (25)$$

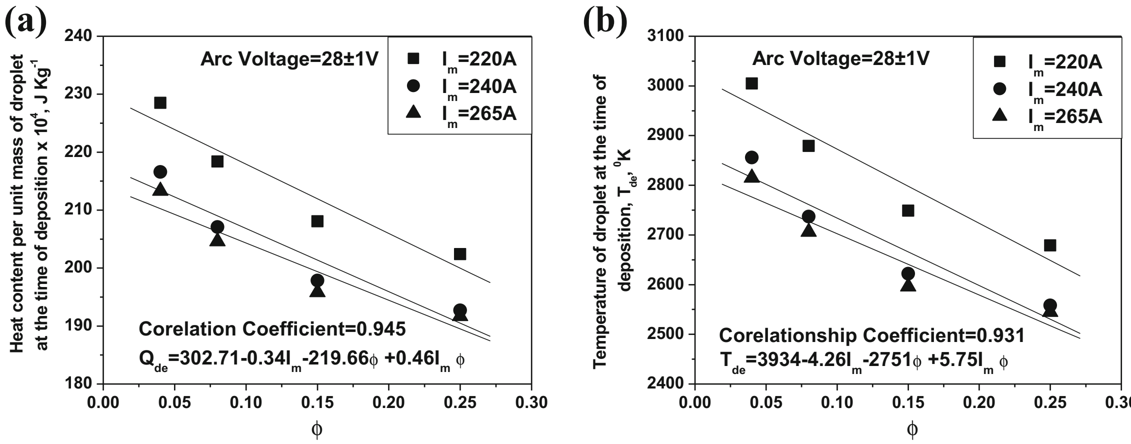

Fig. 4 At a given arc voltage of 28±1 V, the effect of ϕ on **a** heat content per unit mass of droplet and **b** temperature of droplet at the time of deposition at different I_m of 220, 240, and 265 A

The thermal behavior of metal transfer being dictated by ϕ and I_m may affect the total heat transfer to weld pool and its temperature. Thus, the thermal behavior of weld pool has been studied considering total heat transferred to the weld pool (Q_T) and average weld pool temperature (T_{WP}) under different pulse parameters (Table 2).

4.2 Thermal characteristics of weld pool

At a given arc voltage of 28±1 V, the influence of ϕ on estimated Q_T at different mean currents (I_m) of about 220±3, 240±2, and 265±4 A has been depicted in Fig. 6. The figure shows that Q_T reduces with increment of ϕ at a given I_m and enhances with I_m at a given ϕ. The Q_T is primarily dictated by the arc heat transferred to weld pool largely depending upon the effective mean current and heat of filler metal transferred per unit time, which are having similar trend of variation with ϕ at a given I_m and with I_m at a given ϕ (Table 2). The empirical correlation of Q_T with ϕ and I_m at a given arc voltage has been worked out as follows.

$$Q_T = 1,436.45 + 29.19 I_m - 5,801.63\phi + 0.04 I_m \phi + e_{r3} \quad (26)$$

At a given arc voltage of 28±1 V, the effect of ϕ on estimated weld pool temperature (T_{WP}) at a depth of about 2.1–3.5 mm from its surface and about 3.5 mm from arc center under different Ω and I_m have been

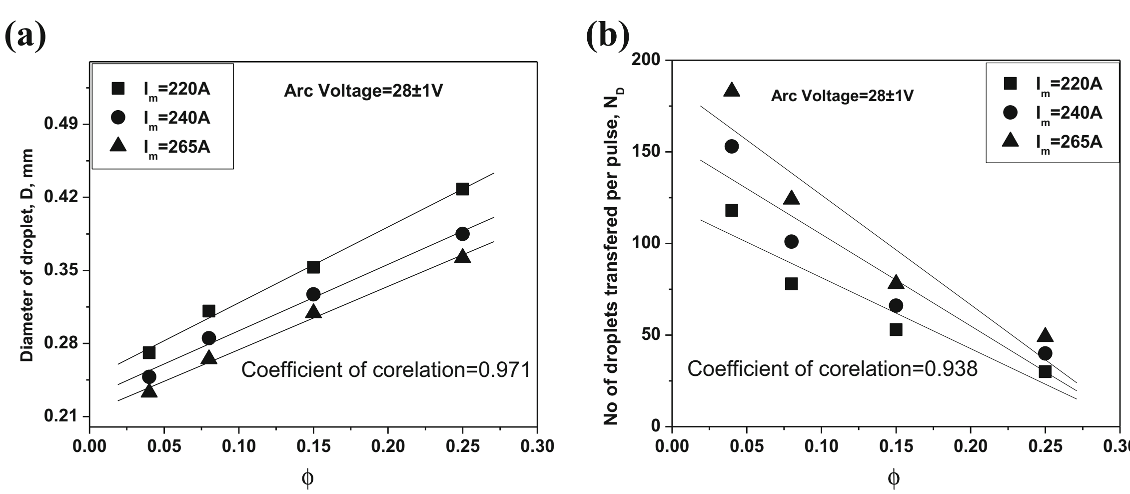

Fig. 5 At a given arc voltage of 28±1 V, the effect of ϕ on **a** diameter of droplet and **b** number of droplet transferred per pulse at different I_m of 220, 240, and 265 A

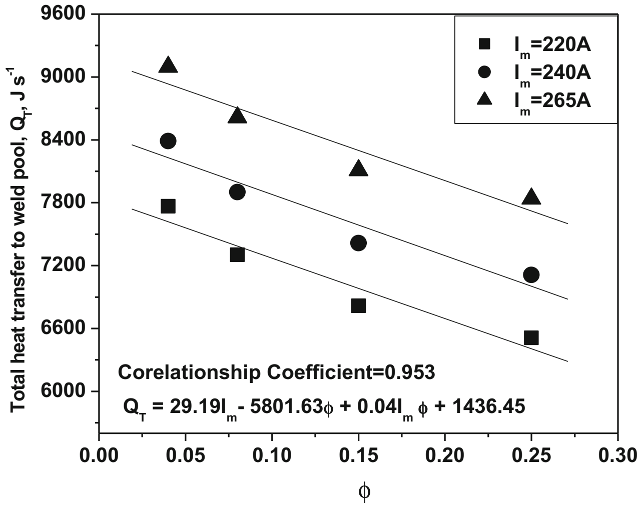

Fig. 6 At a given arc voltage of 28±1 V, the effect of ϕ on total heat transfer to weld pool at different I_m of 220, 240, and 265 A

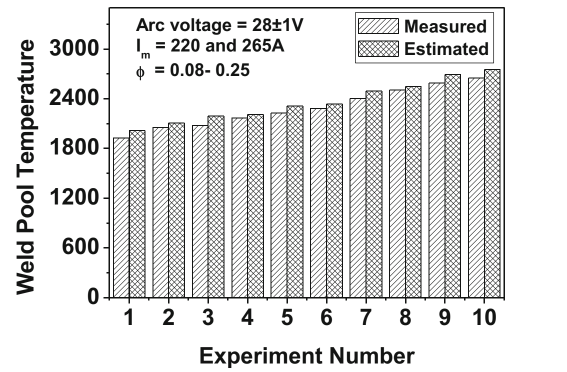

Fig. 8 At a given arc voltage of 28±1 V, comparison of measured and estimated weld pool temperature at depths of about 2.5–3 mm from its weld pool surface at different I_m and ϕ

shown in Fig. 7a–c. It has been observed that at a given Ω and I_m, the T_{WP} reduces significantly with the increase of ϕ. The T_{WP} enhances with the increase of Ω at a given I_m and ϕ and it also increases appreciably with the enhancement of I_m at a given Ω and ϕ. At a given Ω and I_m, the reduction of T_{WP} with the increase of ϕ may have primarily happened due to decrease of

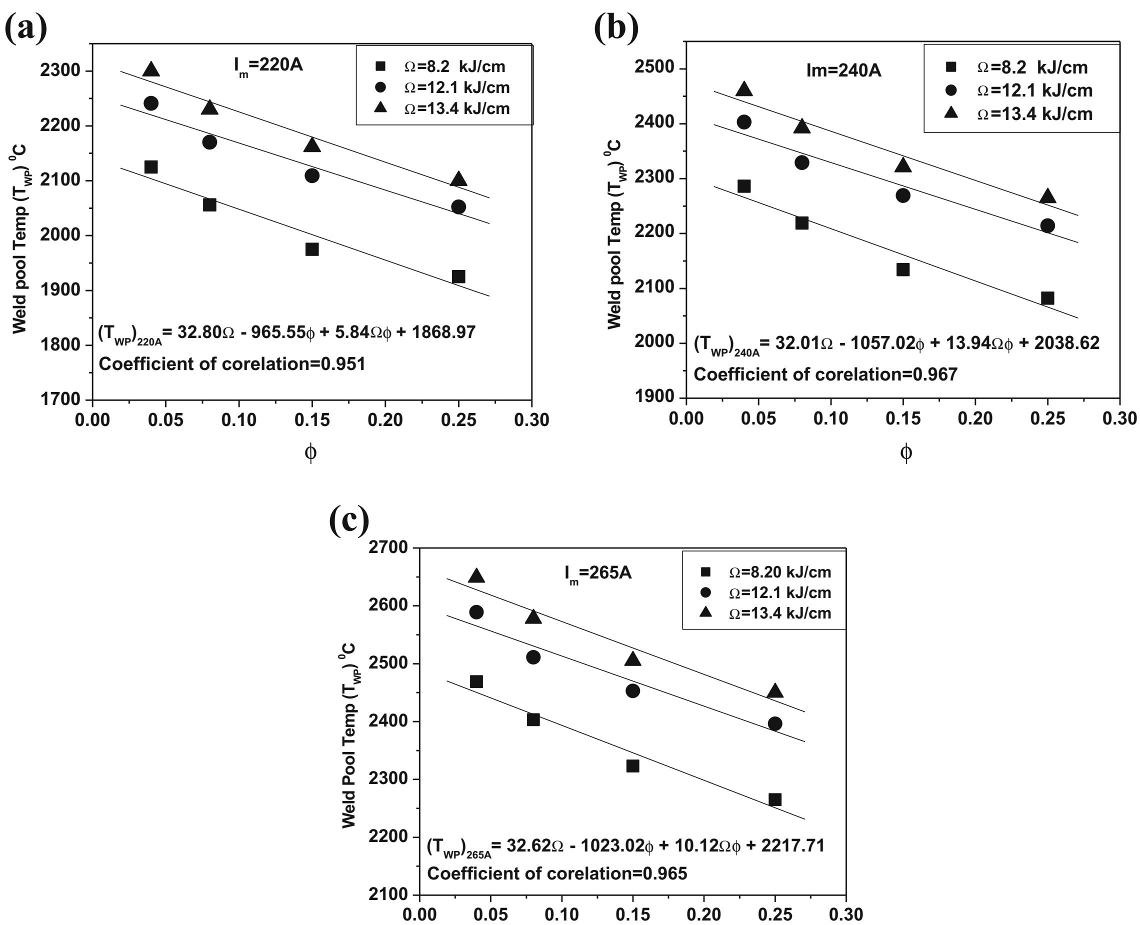

Fig. 7 At a given arc voltage of 28±1 V, the effect of ϕ and Ω on weld pool temperature under different mean current of **a** 220 A; **b** 240 A; and **c** 265 A

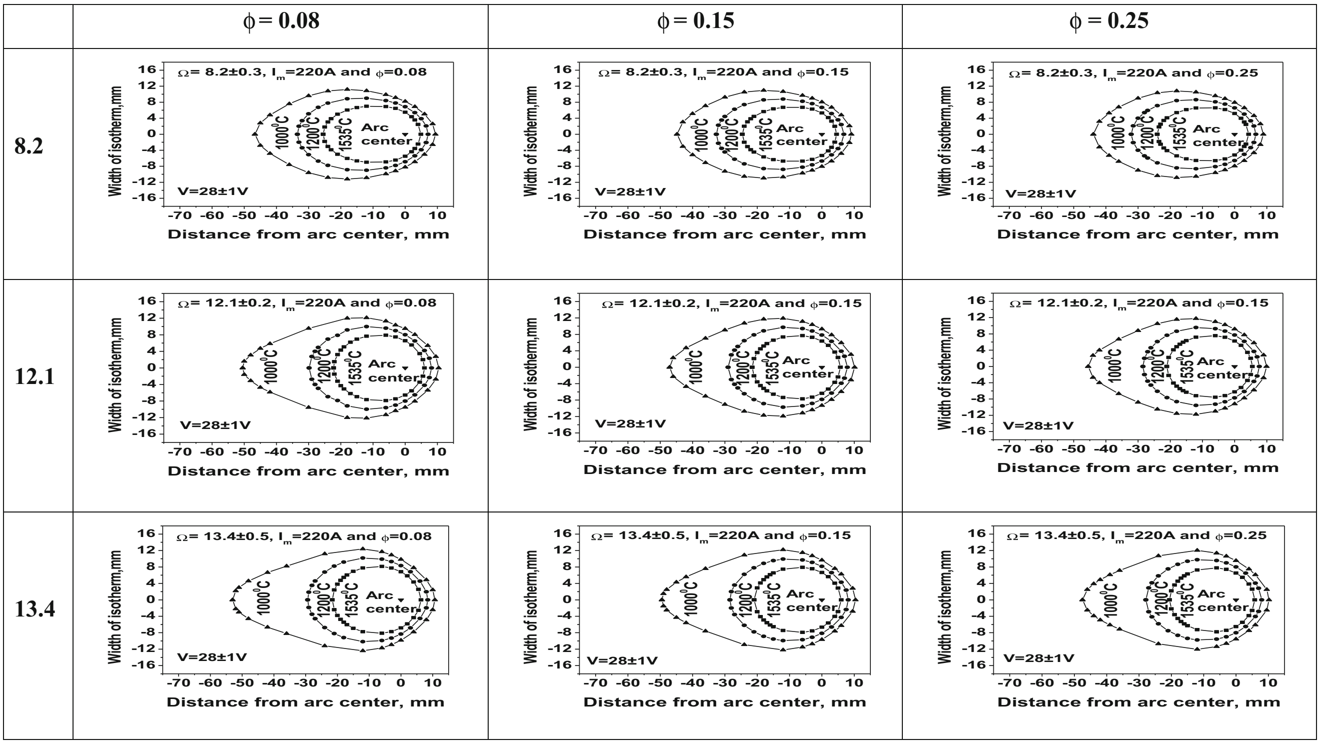

Fig. 9 At a given arc voltage of 28±1 V, the effect of ϕ and Ω on weld isotherm at mean current of 220±3 A

Q_{de} and T_{de} as shown in Fig. 4a and b. The enhancement of T_{WP} with the increase of Ω at a given I_{m} and ϕ is attributed to increase of total heat transferred to the weld pool (Q_{T}) per unit length. However, the

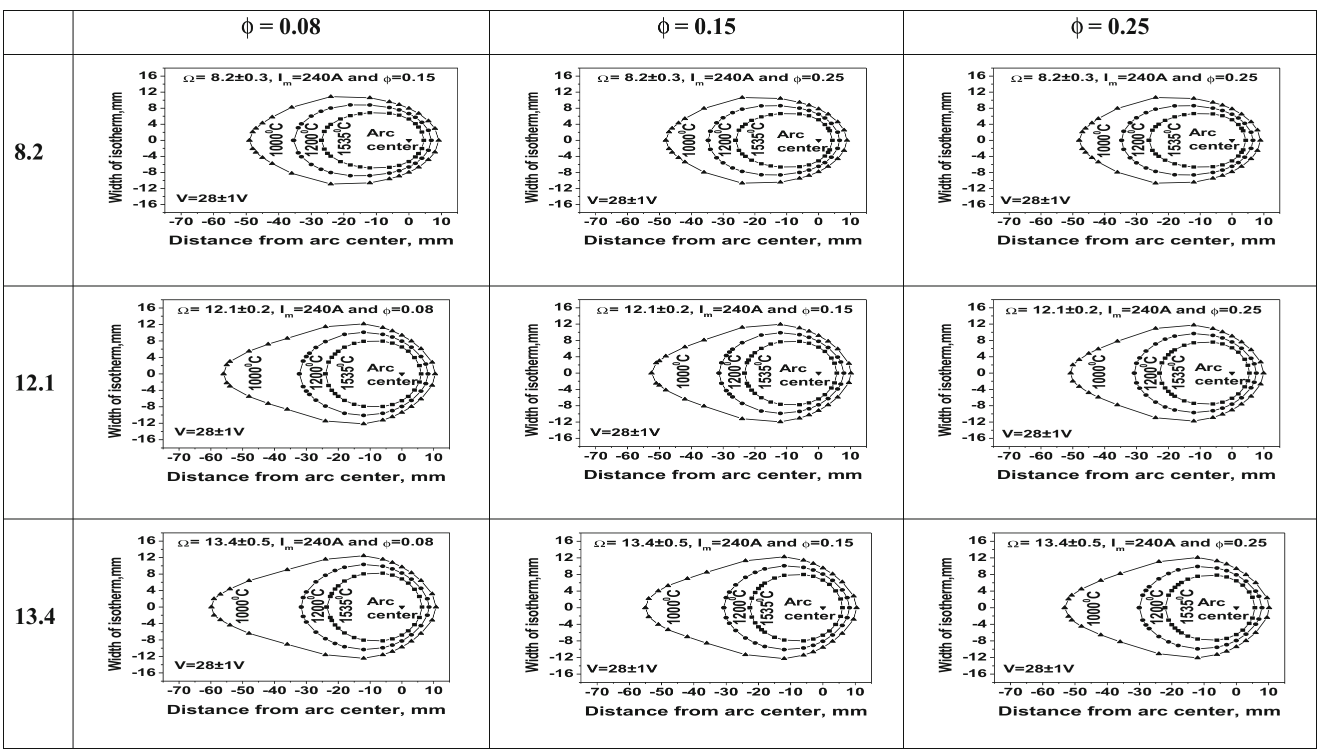

Fig. 10 At a given arc voltage of 28±1 V, the effect of ϕ and Ω on weld isotherm at mean current of 240±2 A

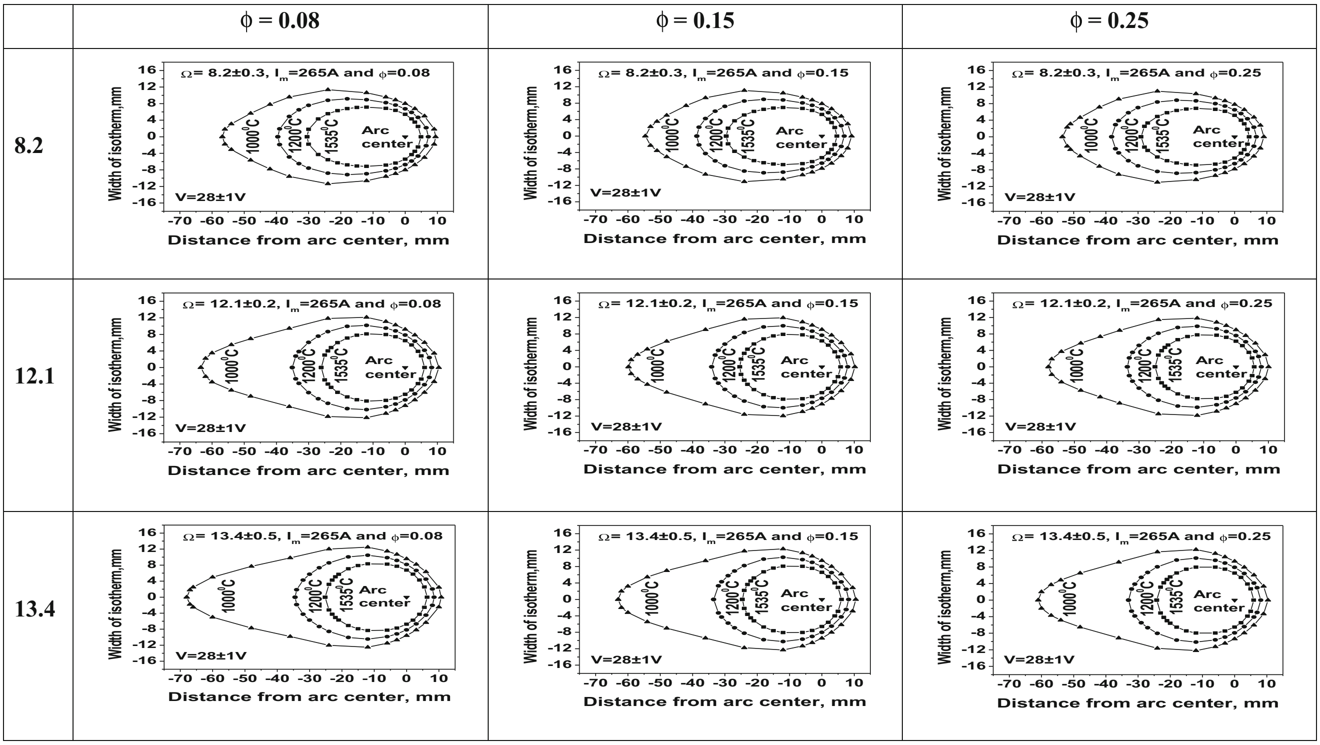

Fig. 11 At a given arc voltage of 28±1 V, the effect of ϕ and Ω on weld isotherm at mean current of 265±4 A

appreciable increment of T_{WP} with the enhancement of I_m at a given Ω and ϕ has primarily happened due to increase of number of droplets transferred per pulse with the increase of I_m. This is because the molten

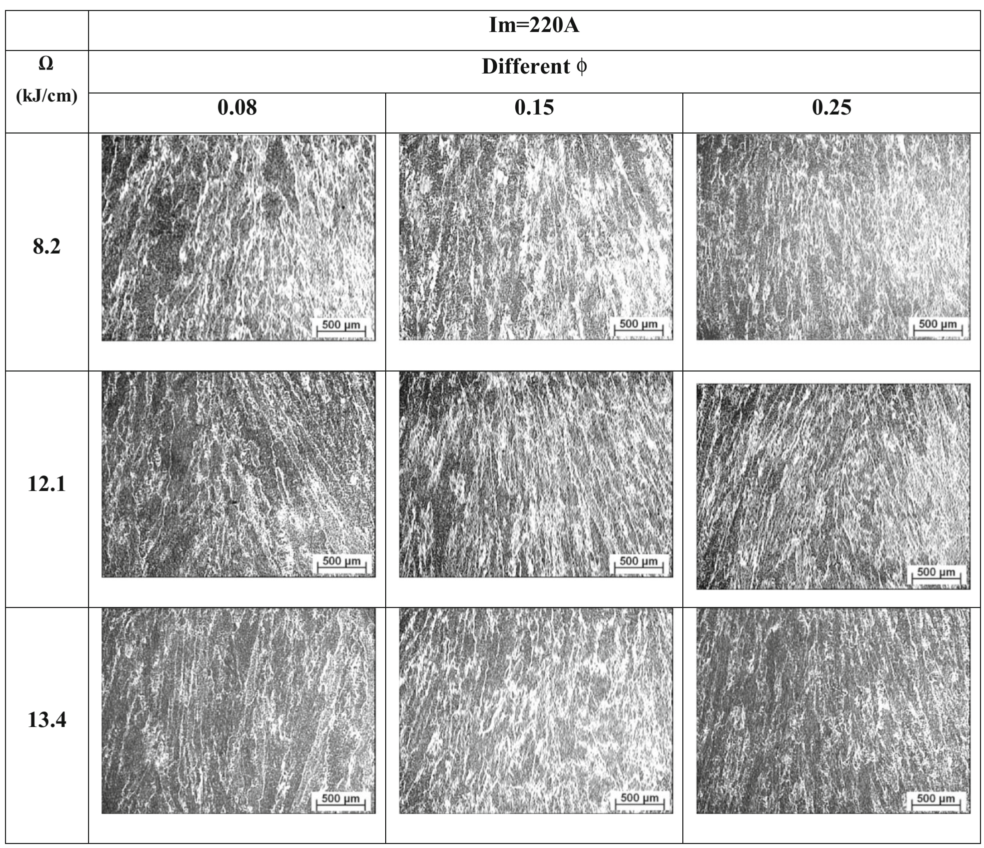

Fig. 12 Typical microstructure of weld deposits showing the effect of ϕ and Ω at a given I_m of 220 A

Fig. 13 Typical microstructure of weld deposits showing the effect of ϕ and Ω at a given I_m of 240 A

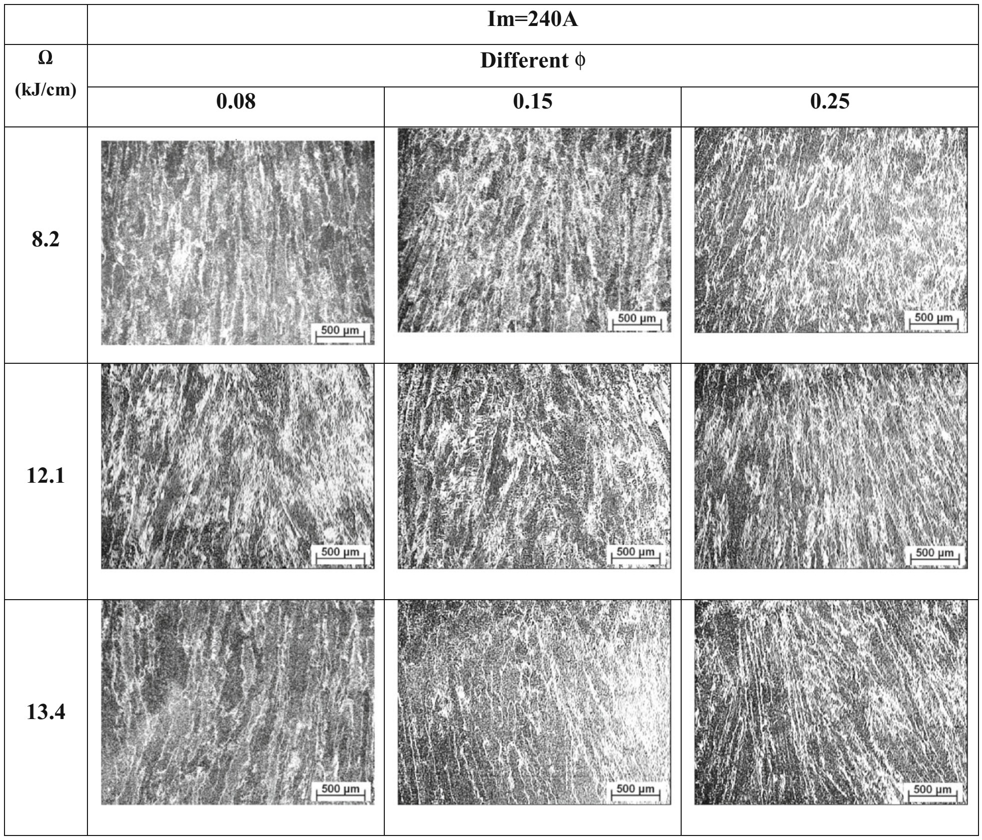

Fig. 14 Typical microstructure of weld deposits showing the effect of ϕ and Ω at a given I_m of 265 A

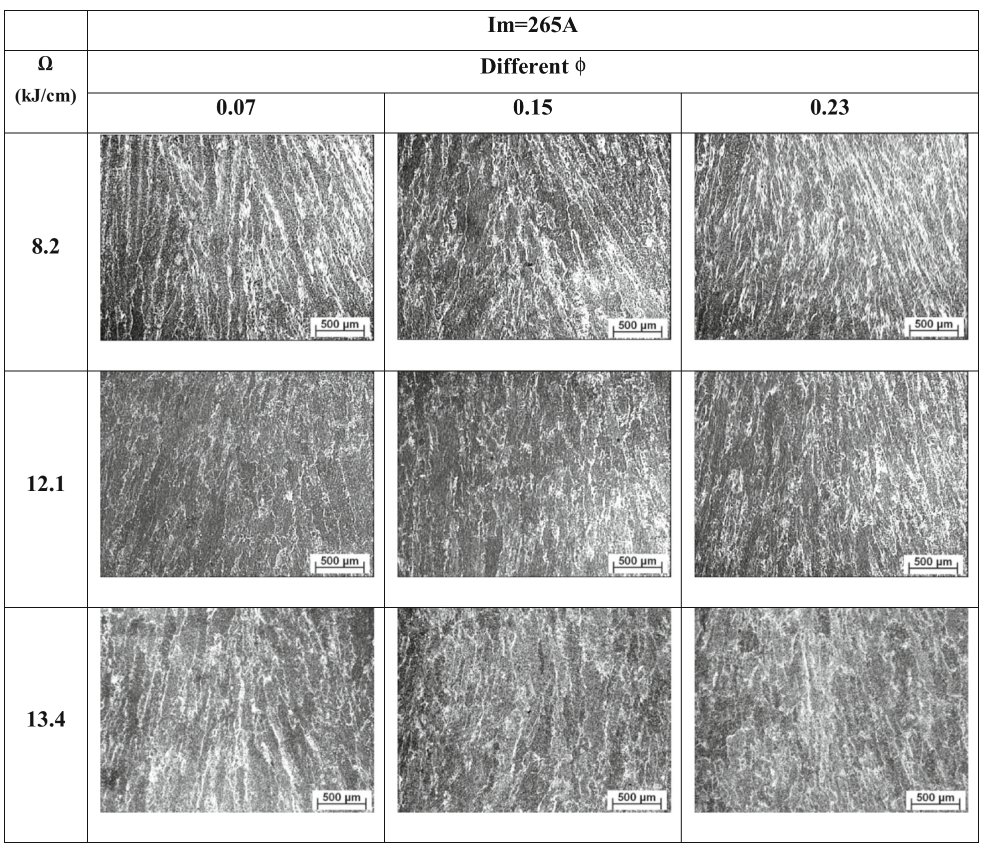

metal droplets carry appreciable amount of heat while getting transferred to weld pool. The empirical correlations of T_{WP} with respect to Ω and ϕ at different I_m of 220, 240, and 265 A have been worked out as follows.

$$(T_{WP})_{220\ A} = 1,868.97 + 32.80\Omega - 965.55\phi + 5.84\Omega\phi + e_{r4} \tag{27}$$

$$(T_{WP})_{240\ A} = 2,038.62 + 32.01\Omega - 1,057.02\phi + 13.94\Omega\phi + e_{r5} \tag{28}$$

$$(T_{WP})_{265\ A} = -2,217.71 + 32.62\Omega - 1,023.02\phi + 10.12\Omega\phi + e_{r6} \tag{29}$$

The mathematical expression (Eq. 8) used for estimation of weld pool temperature has been verified for certain cases by comparing the theoretically estimated values with the experimental measured values. At a given arc voltage of 28±1 V, a comparison of the theoretically estimated and measured values of T_{WP} at depths of about 2.5–3.0 mm from molten pool surface at different pulse parameters has been shown in Fig. 8. It has been observed that estimated values of T_{WP} are in good agreement with their corresponding measured values with a maximum deviation of about ±7–8 %. The limitation of the expression is that it is unable to estimate weld pool temperature correctly close to the arc center within a radius of 2 mm to avoid significant influence of arc heating [15].

The Q_T and T_{WP} as a function of pulse parameters consequently affect the weld isotherm. Thus, it is interesting to study the effect of pulse parameters on weld isotherm in order to critically understand, predict, and control the weld pool up to a maximum extent for its desired performance.

4.3 Weld isotherm

At a given arc voltage of 28±1 V, the effect of ϕ on weld isotherm at different I_m and Ω lying in the range of 220–265 A and 8.2±0.3 to 13.4±0.5 kJ/cm, respectively, have been shown in Figs. 9, 10, and 11. It is observed that the width and length of isotherm decreases with the increase of ϕ at a given I_m and Ω. This is attributed to the reduction in total heat transferred to the weld pool with the increase of ϕ. It has also been observed that the increase of Ω at a given I_m

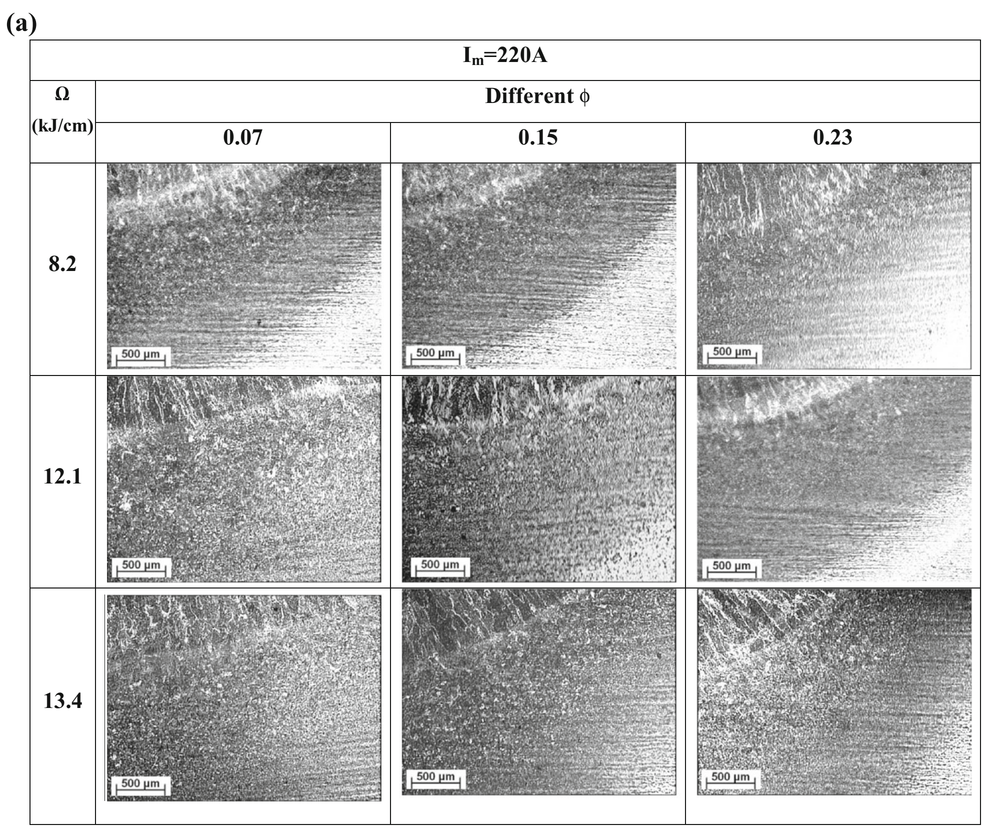

Fig. 15 Typical microstructure of HAZ showing the effect of ϕ and Ω at a given I_m of 220 A at comparatively **a** low and **b** high magnification

(b)

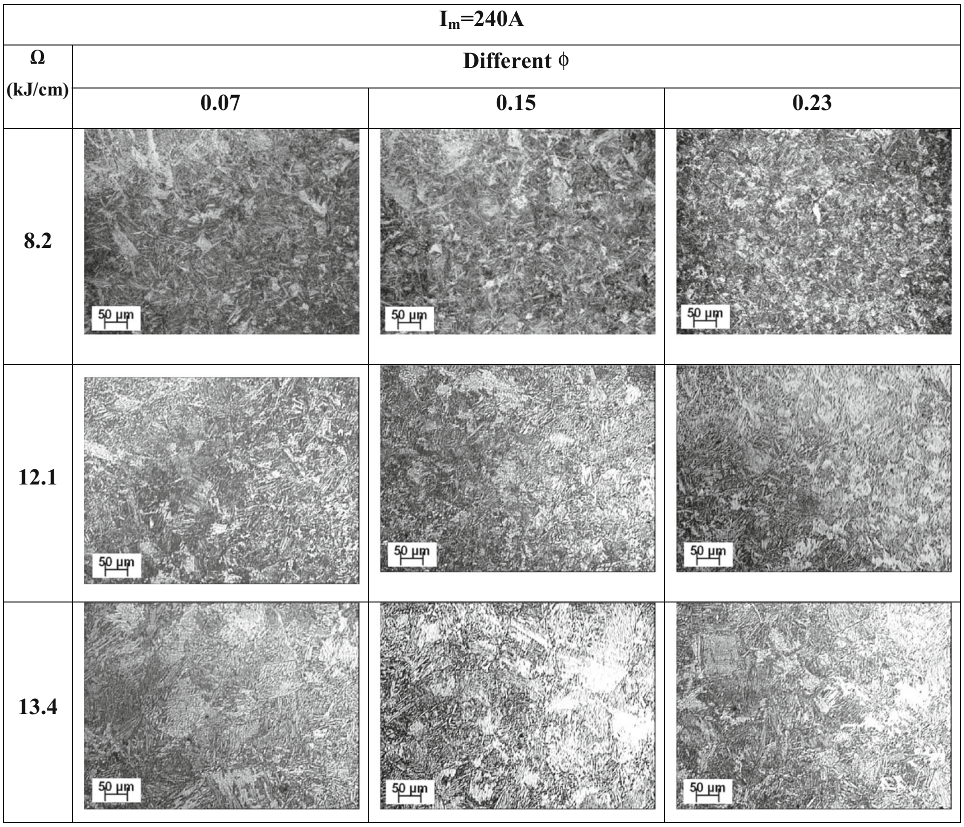

Fig. 15 (continued)

(a)

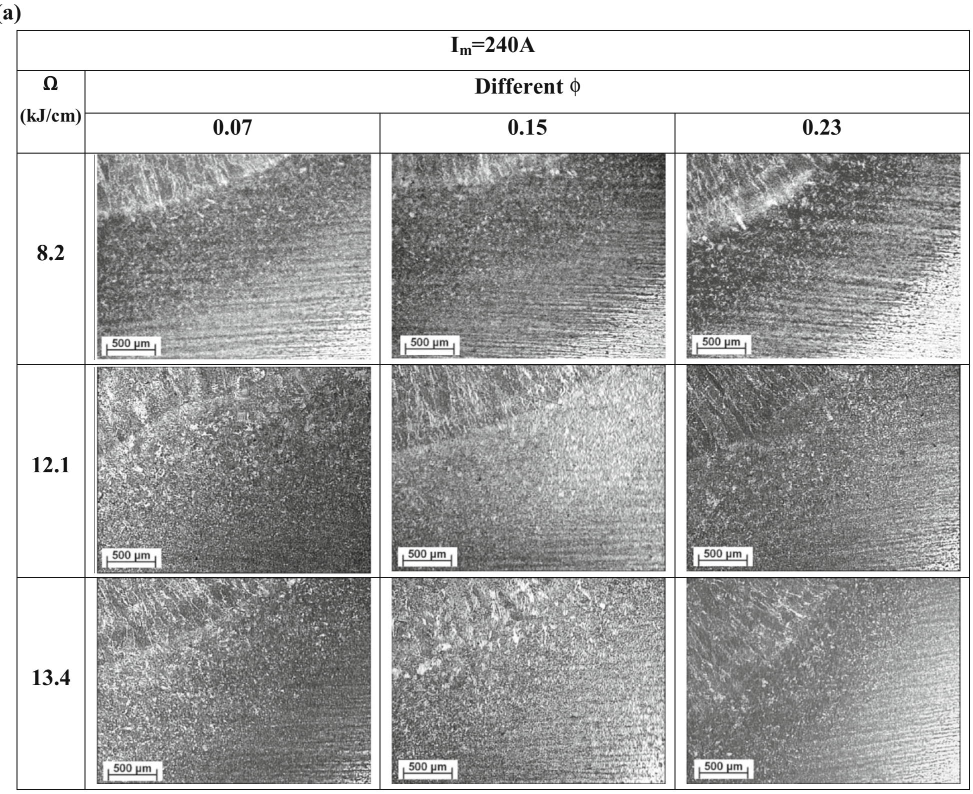

Fig. 16 Typical microstructure of HAZ showing the effect of ϕ and Ω at a given I_m of 240 A at comparatively **a** low and **b** high magnification

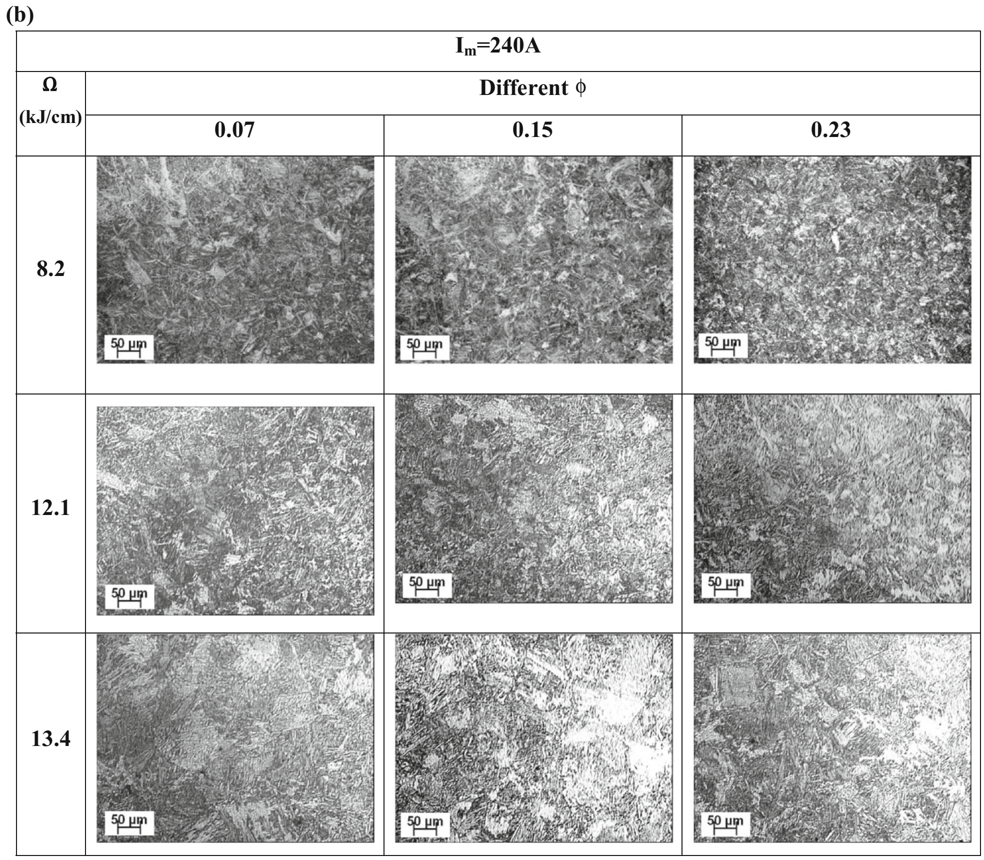

Fig. 16 (continued)

and ϕ and the increase of I_m at a given Ω and ϕ enhance the width of the isotherm. This is attributed to the enhancement of the Q_T and T_{WP} with the increment of Ω and I_m. It is further observed that increase of Ω at a given I_m and ϕ, which is achieved through the reduction of welding speed, decreases the length of the weld pool. This may have primarily happened because of its ability to cool the molten weld pool to relatively higher extent due to availability of comparatively more time at lower welding speed leading to higher Ω. The size of weld isotherm in welding process may affect the microstructure of weld and heat-affected zone resulting into different properties of the weld.

4.4 Microstructure of weld

It is intended to study the effect of welding parameters on microstructure of weld and HAZ in order to realize desired properties of weld through proper control of welding parameters. At a given arc voltage of 28±1 V, the typical variation in microstructure of weld deposit with respect to ϕ at different I_m of 220±3, 240±2, and 265±4 A has been shown in Figs. 12, 13, and 14, respectively, where the Ω lies in the range of 8.2±0.3 to 13.4±0.5 kJ/cm. The weld has been found to consist of dendrite microstructure which is produced under prevailing positive condition of solidification of weld pool at a relatively slow cooling favoring dendritic growth of primary solids. It has been observed that with the increase of ϕ at a given I_m and Ω, the microstructure of weld becomes relatively finer. This is largely attributed to decrease of T_{WP} and application of comparatively milder weld isotherm with the increase of ϕ (Figs. 7, 9, 10, and 11) resulting in enhancement of cooling rate due to increase of conduction and convection heat losses from the weld pool [5]. The figures also reveal that at a given ϕ and arc voltage, the microstructure of weld becomes comparatively coarser with the increase of Ω irrespective of variation of I_m due to the enhancement of T_{WP}. The enhancement of T_{WP} gives rise to development of coarser microstructure due to reduction in the conduction within the weld pool. The figure also shows that at a given ϕ, Ω, and arc voltage, the increase of I_m comparatively coarsens the microstructure of weld due to increase of T_{WP} and application of relatively stronger weld isotherm. This has again happened because of association of lower cooling rate with higher T_{WP} and stronger weld isotherm.

The microstructure of weld deposit at any ϕ, Ω, and I_m have been found to have dendrites consisting of dark pearlite with pro-eutectoid ferrite at the boundary. However, at a given I_m and Ω, the production of comparatively finer microstructure of weld deposit with the increase of ϕ may have caused an enhancement of the area of dendrite boundary resulting into larger amount of pro-eutectoid ferrite in the matrix. This has happened due to association of relatively larger area of dendrite boundary with finer microstructure.

4.5 Microstructure of heat-affected zone

The variation in microstructure of HAZ, such as grain coarsening adjacent to fusion line and width of HAZ, with respect to welding parameters has been studied. In case of weld deposition at a given arc voltage of 28±1 V, the typical variation in microstructure of HAZ adjacent to fusion line with respect to varied ϕ and Ω at different I_m of 220±3, 240±2, and 265±4 A has been shown in Figs. 15, 16, and 17, respectively, at relatively low and high magnifications. The Figs. 15, 16, and 17 qualitatively reveal the extent of variation of grain coarsening in HAZ adjacent to fusion line with respect to welding parameters. The figures also depict that the width of grain coarsening adjacent to the fusion line changes considerably with the change in ϕ, Ω, and I_m. It has been found that the microstructure close to fusion line primarily consists of bainite and acicular ferrite as confirmed by their morphology and matrix hardness lying in the range of 219 and 338 VHN, respectively.

The figures also show that at a given Ω, the microstructure of HAZ adjacent to the fusion line becomes comparatively finer with the increase of ϕ irrespective of variation of I_m. This might have happened because the increase of ϕ reduces the heat transfer to the weld pool as well as the size of weld isotherm and thus enhances the cooling rate of HAZ. The figure further reveals that at a given ϕ and I_m, the increase of Ω relatively coarsens the microstructure of HAZ adjacent to the fusion line. This has been primarily happened because a higher Ω enhances the Q_T and results in application of stronger weld isotherm, which may increase the temperature of HAZ and

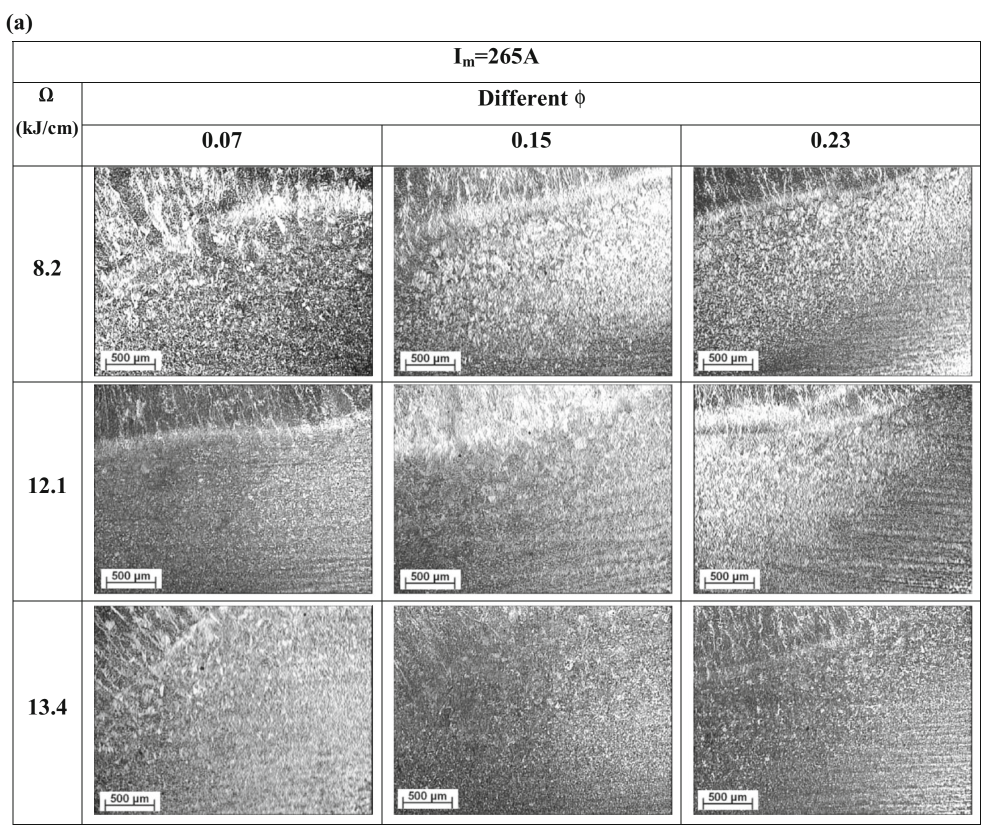

Fig. 17 Typical microstructure of HAZ showing the effect of ϕ and Ω at a given I_m of 265 A at comparatively **a** low and **b** high magnification

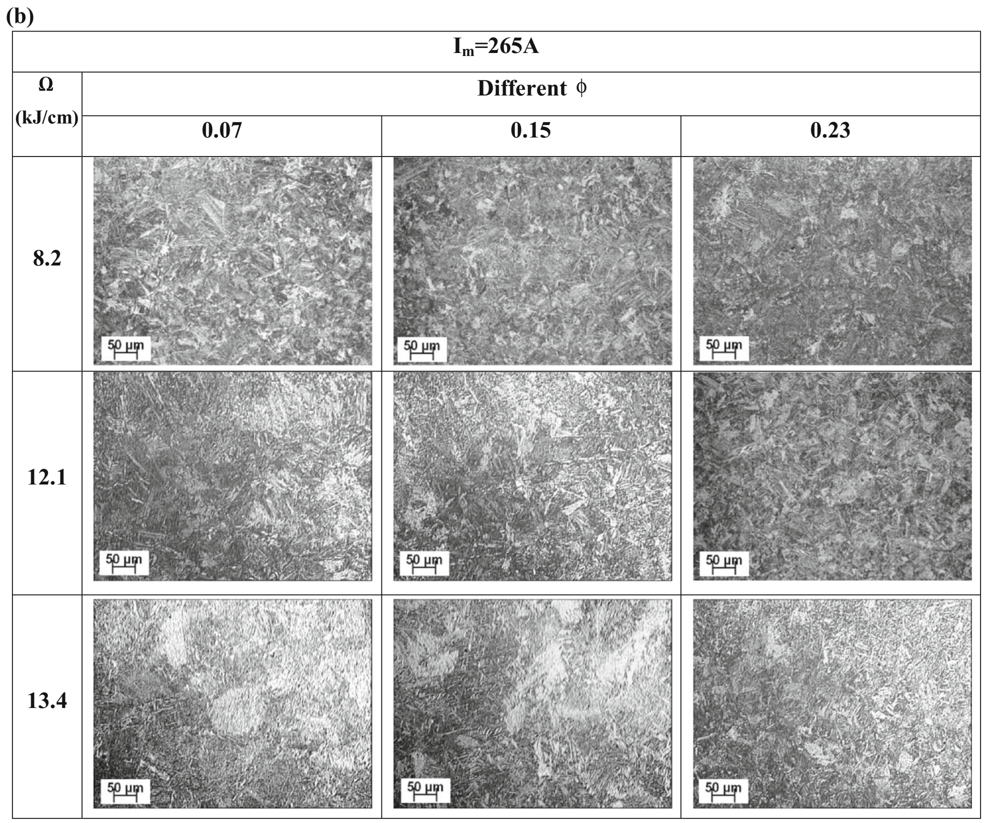

Fig. 17 (continued)

reduce the cooling rate resulting in development of comparatively coarser microstructure. In addition to this, it is also observed that at a given ϕ and Ω, the increase of I_m comparatively coarsens the microstructure of HAZ adjacent to the fusion line because a higher I_m enhances the temperature of the droplets transferred to the weld pool finally attributing to increase of temperature of the HAZ. The microstructure close to fusion line primarily consists of bainite within the prior austenite grains having grain boundary ferrite. The amount of grain boundary ferrite has been found to reduce with the enhancement of ϕ as the microstructure becomes relatively finer.

The change in characteristics of HAZ has been studied by measuring the width of HAZ and grain coarsening adjacent to fusion line. At a given arc voltage of 28±1 V, the variation of measured width of HAZ adjacent to the fusion line with respect to ϕ, at different I_m of 220±3, 240±2, and 265±4 A, has been shown in Fig. 18a–c, respectively, where the Ω has been varied within 8.2±0.3 to 13.4±0.5 kJ/cm. The figures show that at a given Ω and I_m, the width of HAZ decreases with the increase of ϕ. It has been further observed that at a given ϕ and I_m, the increase in Ω, and at a given ϕ and Ω, the increase in I_m, enhance the width of HAZ. Such a variation in the width of HAZ with change of ϕ, Ω, and I_m might have happened largely due to the variation in Q_T and weld isotherm resulting in change of temperature of HAZ. The empirical correlations of width of HAZ with Ω and ϕ at different I_m are as follows.

$$(W_{\mathrm{HAZ}})_{220} = 1,679.185 + 47.657\Omega - 616.063\phi - 17.309\Omega\phi + e_{r7} \tag{30}$$

$$(W_{\mathrm{HAZ}})_{240} = 1,701.182 + 54.652\Omega - 288.217\phi - 44.146\Omega\phi + e_{r8} \tag{31}$$

$$(W_{\mathrm{HAZ}})_{265} = 1,849.573 + 53.921\Omega - 93.995\phi - 63.959\Omega\phi + e_{r9} \tag{32}$$

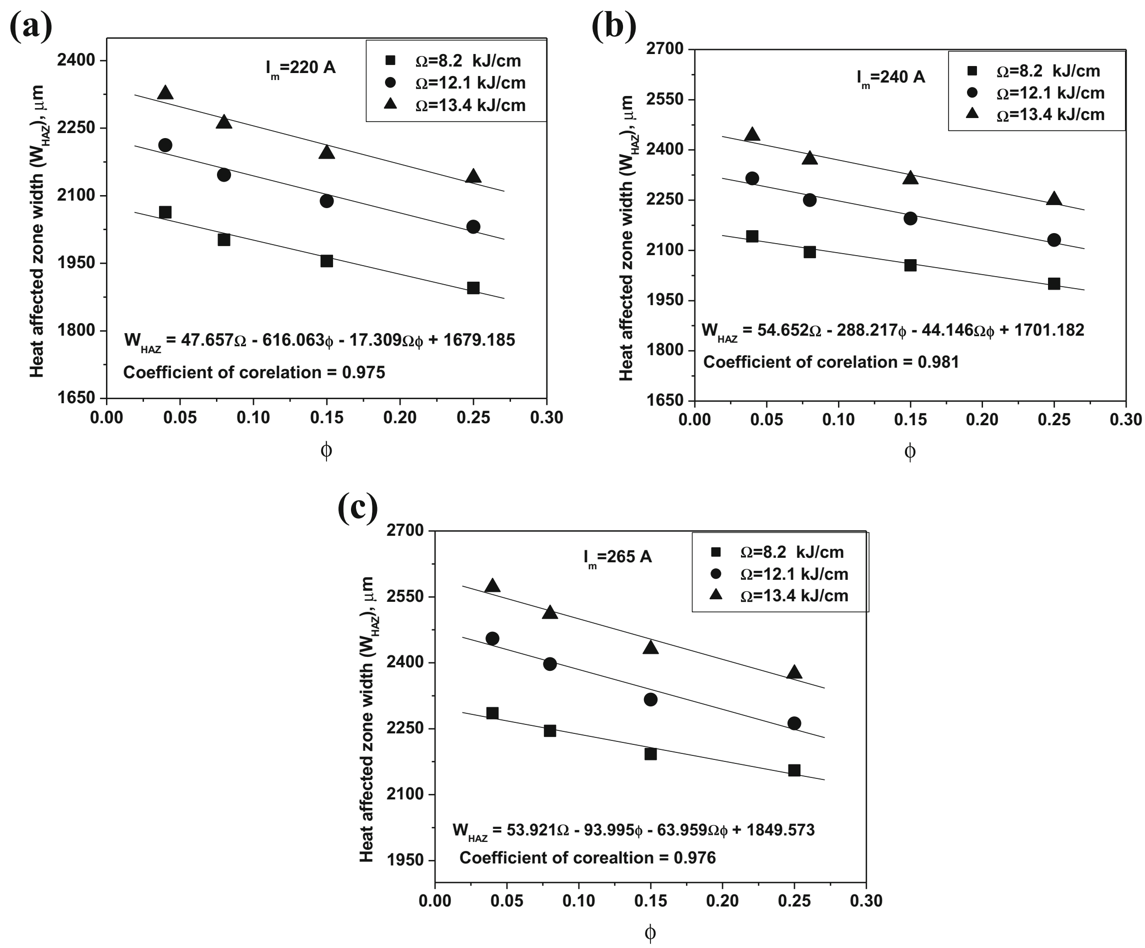

Fig. 18 At a given arc voltage of 28±1 V, the effect of ϕ and Ω on width of HAZ under different mean current of **a** 220 A; **b** 240 A; and **c** 265 A

At a given arc voltage of 28±1 V, the variation of measured average grain size of HAZ adjacent to fusion line lying within the range of 0.3−1 mm with respect to ϕ at different I_m of 220±3, 240±2, and 265 ±4 A, under varying Ω of 8.2±0.3 to 13.4±0.5 kJ/cm, has been shown in Fig. 19a–c, respectively. The figures illustrate that at a given Ω and I_m, the grain size of HAZ adjacent to fusion line decreases with the increase of ϕ. The figures also depict that at a given ϕ and I_m, the increase in Ω, and at a given ϕ and Ω, the increase in I_m, considerably enhance the grain size of HAZ. The variation in grain size with the change in ϕ, Ω, and I_m is attributed to the changes in Q_T, cooling rate of HAZ, and application of weld isotherm. The variation in microstructure of weld and HAZ with respect to pulse parameters significantly affects their properties as it is noted during studies on their hardness.

4.6 Hardness of weld and heat-affected zone

The effect of variation in ϕ, Ω, and I_m on hardness of weld pool (H_{WP}) as well as coarse grain region of HAZ (H_{CGHAZ}) near fusion line lying within the range of 0.7–0.8 mm is shown in Figs. 20 and 21, respectively. The figures reveal that the hardness of the weld pool at any ϕ, Ω, and I_m is relatively more than that of the base metal (178±6 VHN), which might have largely happened due to change in the microstructure and chemical composition of the weld pool. The variation in microstructure of weld might have taken place due to change of its chemical composition owing to dilution of weld deposit by the fusion of base metal and variation in rate of solidification primarily governed by the rate of cooling as a function of the geometry of base plate fusion and amount of weld deposit with its extent of super heating at different pulse parameters. It

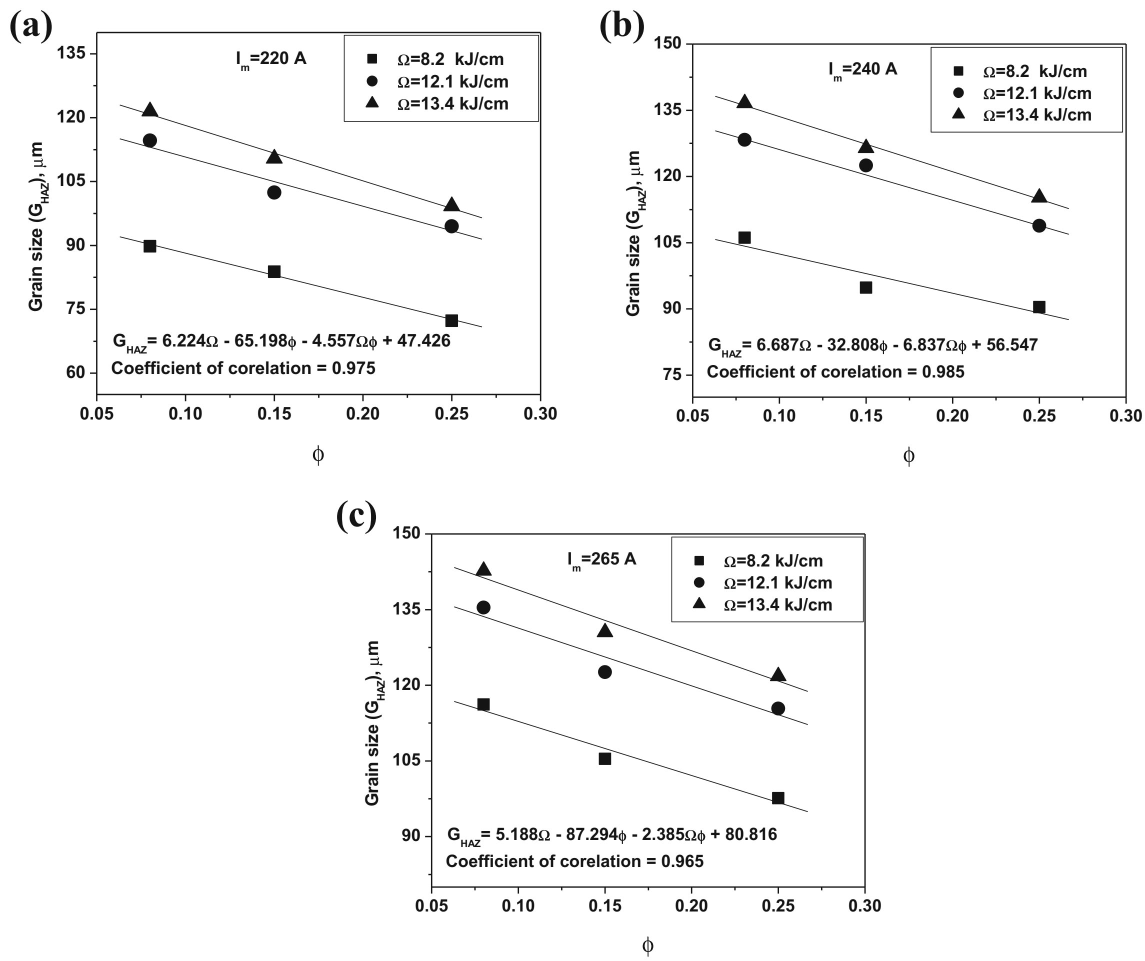

Fig. 19 At a given arc voltage of 28±1 V, the effect of ϕ and Ω on average grain size of HAZ near to fusion line within the range of 0.3–1 mm under different mean current of **a** 220 A; **b** 240 A; and **c** 265 A

is also observed that hardness of the HAZ at any ϕ, Ω, and I_m is comparatively more than that of the base metal (178±6 VHN) as well as weld pool. This has been primarily happened because of re-crystallization and changes in phases which are the function of chemical composition and cooling rate depending upon Q_T and T_{WP} governed by the welding parameters [9]. This has primarily happened as a result of a combined influence of re-crystallization and phase transformation in HAZ primarily dictated by its thermal cycle depending upon Q_T and T_{WP} as a function of the welding parameters [9]. The figures further show that at a given I_m and Ω, the hardness of weld pool as well as HAZ increases significantly with the increase of ϕ. The increase of hardness of weld pool with the enhancement of ϕ may be primarily attributed to reduction of Q_T and enhancement of cooling rate resulting in production of comparatively harder phases and finer microstructure. This is primarily realized from the matrix morphology and its hardness, which is well in agreement to the earlier observation on HSLA steel [26], wherein it was found that there is formation of relatively harder phases in the weld, the extent of which depends upon carbon content and cooling rate. The formation of such phase is further enhanced by favorable heat sink provided by the base metal. While the increase of hardness of HAZ with the enhancement of ϕ may be governed by relatively lower temperature of HAZ because of lower Q_T and relatively higher carbon content of base metal with production of relatively finer microstructure due to enhanced cooling rate as shown by lower average grain size adjacent to the

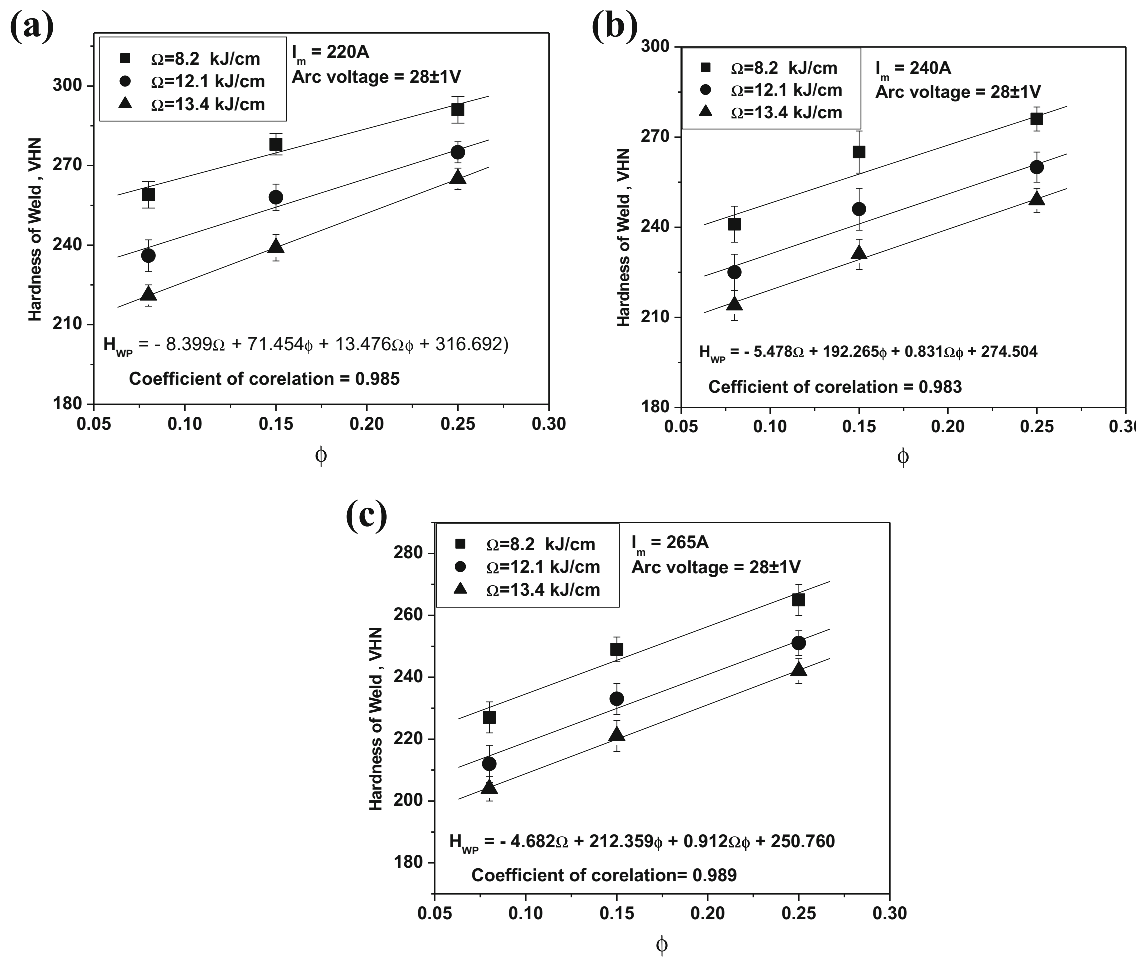

Fig. 20 At a given arc voltage of 28±1 V, the effect of ϕ and Ω on hardness of weld pool under different mean current of **a** 220 A; **b** 240 A; and **c** 265 A

fusion line of HAZ (Fig. 19). Accordingly, the microstructure of the HAZ may contain some amount of martensite leading to comparatively higher hardness [26]. The figure further depicts that at a given ϕ and I_m, the increase of Ω, and at a given ϕ and Ω, the increase of I_m, decrease the hardness of weld pool as well as HAZ. The reduction in hardness of weld pool and HAZ with the increase of Ω and I_m may be largely attributed to the production of relatively coarser microstructure of weld pool and HAZ, respectively, as shown by the average grain size of HAZ. This has occurred due to relatively lower heat transfer to the weld pool and application of weaker weld isotherm giving rise to lower cooling rate with enhancement of I_m, or Ω, keeping other pulse parameters same. The changes in heat transfer to weld pool also affect the peak temperature of HAZ affecting accordingly its cooling rate. The empirical correlations of hardness of weld pool and HAZ with respect to ϕ and Ω at different I_m have been worked out as follows.

$$(H_{\mathrm{WP}})_{220} = 316.692 - 8.399\Omega + 71.454\phi + 13.476\Omega\phi + e_{r10} \quad (33)$$

$$(H_{\mathrm{WP}})_{240} = 274.504 - 5.478\Omega + 192.265\phi + 0.831\Omega\phi + e_{r11} \quad (34)$$

$$(H_{\mathrm{WP}})_{265} = 250.760 - 4.682\Omega + 212.359\phi + 0.912\Omega\phi + e_{r12} \quad (35)$$

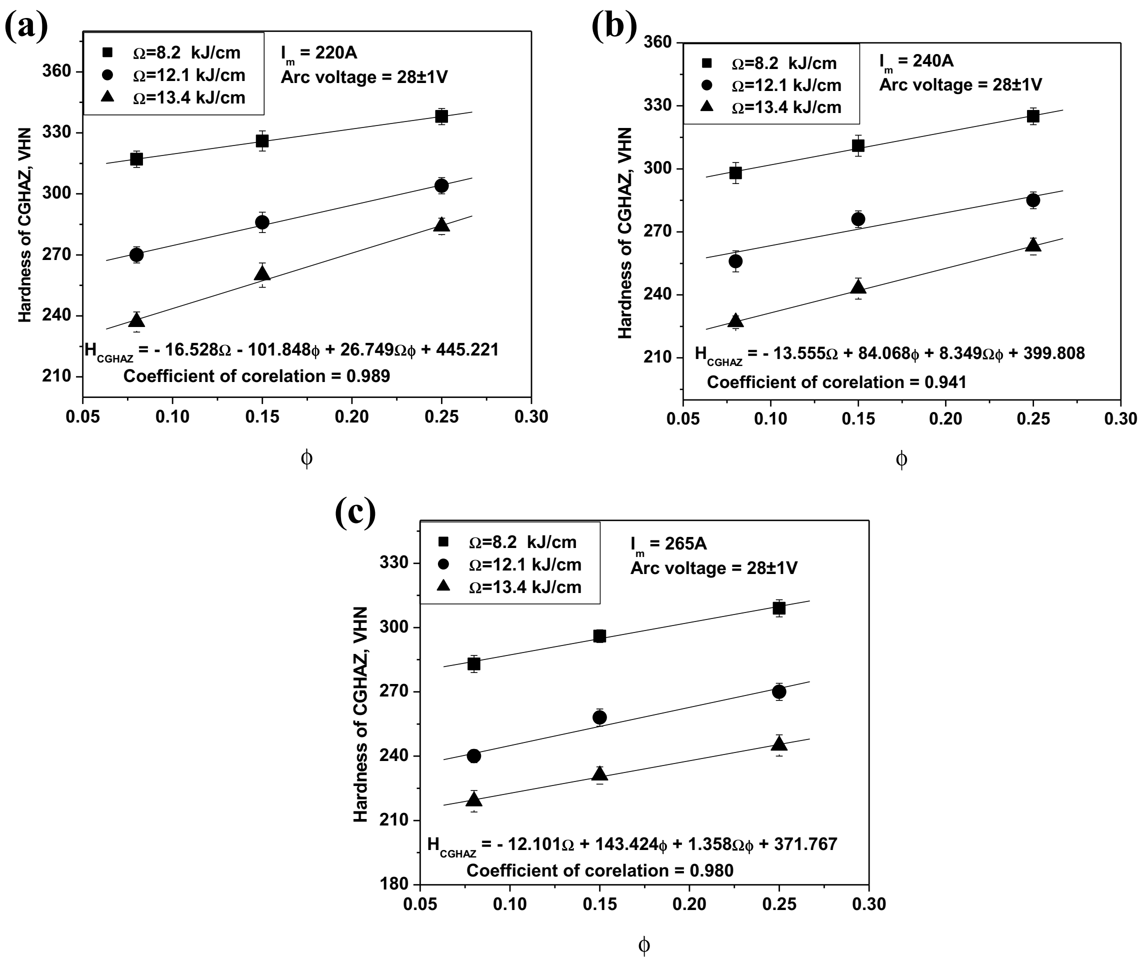

Fig. 21 At a given arc voltage of 28±1 V, the effect of ϕ and Ω on hardness of CGHAZ under different mean current of **a** 220 A; **b** 240 A; and **c** 265 A

$$(H_{\mathrm{CGHAZ}})_{220} = 445.221 - 16.528\Omega - 101.848\phi + 26.749\Omega\phi + e_{r13} \quad (36)$$

$$(H_{\mathrm{CGHAZ}})_{240} = 399.808 - 13.555\Omega + 84.068\phi + 8.349\Omega\phi + e_{r14} \quad (37)$$

$$(H_{\mathrm{CGHAZ}})_{265} = 371.767 - 12.101\Omega + 143.424\phi + 1.358\Omega\phi + e_{r15} \quad (38)$$

The last terms of e_r in Eqs. 24–38 are the experimental error.

5 Conclusions

The effect of summarized influence of pulse parameters, defined by a dimensionless factor ϕ, on thermal characteristics of weld using bead on plate weld deposition of HSLA steel at varied pulse parameters of P-GMAW process has been studied with some interesting observations which may be primarily concluded as follows.

1. At a given heat input Ω, the heat transferred to the weld pool (Q_T) and weld isotherm significantly vary with a change in the factor ϕ and mean current I_m due to its appreciable influence on varying mass, velocity, and heat content of the droplet at the time of deposition.
2. The analytically estimated weld pool temperature (T_{WP}) of the P-GMA weld deposit of HSLA steel lies well within a range of 7 to 8 % variation from the measured value.
3. The microstructures of the weld and HAZ are significantly administered by the factor ϕ and I_m, and it affects their properties. A relatively higher value of ϕ and comparatively lower values of I_m and Ω as well as application of milder weld isotherm result into comparatively finer microstructure and hardness of the weld and HAZ.

References

1. Ghosh PK, Devakumaran K, Pramanick AK (2010) Effect of pulse current on shrinkage stress and distortion in multipass GMA welds of different groove sizes. Weld J 89(3):43-s–53-s
2. Ghosh PK, Devakumaran K, Bhaskarjyoti S (2009) Arc efficiency in pulsed current gas metal arc welding of ferrous and non-ferrous metals. Australas Weld J 54:38–48
3. Praveen P, Yarlagadda PK, Kang MJ (2005) Advancements in pulse gas metal arc welding. J Mater Process Technol 164–165:1113–1119. doi:10.1016/j.jmatprotec.2005.02.100
4. Quintino L, Alllum CJ (1984) Pulsed GMAW: interactions between process parameters, part I. Weld Met Fabr 16(4):126–129
5. Devkumaran K, Ghosh PK (2009) Thermal characteristics of weld and HAZ during pulse current gas metal arc weld bead deposition on HSLA steel plate. Mater Manuf Process Tailor Francis 25(07):616–630. doi:10.1080/10426910903229347
6. Kulkarni SG (2008) Narrow gap pulse current gas metal arc welding of thick wall 304LN stainless steel pipe. Thesis, Indian Institute of Technology, Roorkee, India, pp.1-276
7. Ghosh PK, Dorn L, Goecke SF (2001) Universality of co-relationships among pulse parameters for different MIG welding power sources. Int J Join Mater 13(2):40–47
8. Ghosh PK, Dorn L, Devakumaran K, Hofmann F (2009) Pulsed current gas metal arc welding under different shielding and pulse parameters; part-1: arc characteristics. ISIJ Int 49(2):251–260. doi:10.2355/isijinternational.49.251
9. Ghosh PK, Dorn L, Devakumaran K, Hofmann F (2009) Pulsed current gas metal arc welding under different shielding and pulse parameters; part-2: behaviour of metal transfer. ISIJ Int 49(2):261–269. doi:10.2355/isijinternational.49.261
10. Goyal VK, Ghosh PK, Saini JS (2007) Process controlled micro-structure and cast morphology of dendrite in pulsed current gas metal arc weld deposits of aluminium and Al-Mg alloy. Metall Mater Trans A 38(8):1794–1805. doi:10.1007/s11661-007-9217-3
11. Ghosh PK, Kulkarni SG, Kumar M, Dhiman HK (2007) Pulsed current GMAW for superior weld quality of austenitic stainless steel sheet. ISIJ Int 47(1):138–145. doi:10.2355/isijinternational.47.138
12. Joseph A, Farson D, Harwig D, Richardson R (2005) Influence of GMAW-P current waveforms on heat input and weld bead shape. Sci Technol Weld Join 10(3):311–318. doi:10.1179/174329305X40624
13. Murugan N, Parmar RS (1994) Effect of MIG process parameters on the geometry of the bead in the automatic surfacing of stainless steel. J Mater Process Technol 41:381–398. doi:10.1016/0924-0136(94)90003-5
14. Robert W, Jr M (1999) Principles of welding. Wiley, New York, pp 1–662
15. Goyal VK, Ghosh PK, Saini JS (2008) Analytical studies on thermal behavior and geometry of weld pool in pulsed current gas metal arc welding. J Mater Process Technol 209:1318–1336. doi:10.1016/j.jmatprotec.2008.03.035
16. Lancaster JF (1999) Metallurgy of welding. Abington, Cambridge CBI 6AH England, pp 1–446
17. Roshanthal D, Cambridge M (1946) The theory of moving sources of heat and its application to metal treatments. Trans ASME 68:849–865
18. Radaij D (1992) Heat effects on welding. Springer, New York, pp 1–348
19. Agrawal BP, Ghosh PK (2010) Thermal modeling of multi pass narrow gap pulse current GMA welding by single seam per layer deposition techniques. Mater Manuf Process 25(11):1251–1268. doi:10.1080/10426914.2010.489593
20. Ghosh PK, Goyal VK, Dhiman HK, Kumar M (2006) Thermal and metal transfer behaviour in pulsed current GMA weld deposition of Al-Mg alloy. Sci Technol Weld Join 11(2):232–242. doi:10.1179/174329306X89251
21. Joseph A, Harwig D, Farson DF, Richardson R (2003) Measurement and calculation of arc power and heat transfer efficiency in pulsed gas metal arc welding. Sci Technol Weld Join 8(6):400–406. doi:10.1179/136217103225005642
22. Nguyen NT, Ohta A, Matsuoka K, Suzuki N, Maeda Y (1999) Analytical solution for transient temperature of semi-infinite body subjected to 3-D moving heat source. Weld J 78(8):265-s–274-s
23. Nguyen NT, Mai YW, Simpson S, Ohta A (2004) Analytical approximate solution for the double ellipsoidal heat source in finite thick plate. Weld J 83(3):82s–93s
24. Goyal VK, Ghosh PK, Saini JS (2008) Influence of pulse parameters on characteristics of bead on plate weld deposits of aluminium and its alloy in the pulsed gas metal arc welding processes. Metall Mater Trans A 39A:3260–3275. doi:10.1007/s11661-008-9637-8
25. Abbaschian R, Abaschian L, Reed Hill R (2009) Physical metallurgy principles, 4th edn. Cengage Learning, Stamford, CT, pp 178–180
26. Moon DW, Fonda RW, Spanos G (2000) Micro hardness variation in HSLA 100 steel welds fabricated with new ultra low carbon weld consumables. Weld J 278s–285s, doi: 10.1007/s 11661-001-0179-6